Mass function and dynamical study of the open clusters Berkeley 24 and Czernik 27 using ground based imaging and Gaia astrometry

D. Bisht,[1,2]★ R. K. S. Yadav,[3]★ Shashikiran Ganesh,[1]★ A. K. Durgapal,[4] G. Rangwal[4] and J. P. U. Fynbo[5]

[1] *Physical Research Laboratory, Ahmedabad 380009, India*
[2] *Key Laboratory for Researches in Galaxies and Cosmology, Universityof Science and Technology of China, Chinese Academy of Sciences, Hefei, Anhui 230026, China*
[3] *Artabhatta Research Institute of Observational Sciences, Manora Peak, Nainital 263129, India*
[4] *Department of physics, DSB campus, Kumayun University, Nainital 263001, India*
[5] *The Cosmic Dawn Center, Niels Bohr Institute, Copenhagen University, Juliane Maries Vej 30, DK-2100 Copenhagen Ø, Denmark; DTU-Space Technical University of Denmark, Elektrovej 327, DK-2800, Kongens Lyngby, Denmark*

ABSTRACT

We present a *UBVI* photometric study of the open clusters Berkeley 24 (Be 24) and Czernik 27 (Cz 27). The radii of the clusters are determined as $2\overset{'}{.}7$ and $2\overset{'}{.}3$ for Be 24 and Cz 27, respectively. We use the Gaia Data Release 2 (GDR2) catalogue to estimate the mean proper motions for the clusters. We found the mean proper motion of Be 24 as 0.35 ± 0.06 mas yr^{-1} and 1.20 ± 0.08 mas yr^{-1} in right ascension and declination for Be 24 and -0.52 ± 0.05 mas yr^{-1} and -1.30 ± 0.05 mas yr^{-1} for Cz 27. We used probable cluster members selected from proper motion data for the estimation of fundamental parameters. We infer reddenings $E(B - V) = 0.45 \pm 0.05$ mag and 0.15 ± 0.05 mag for the two clusters. Analysis of extinction curves towards the two clusters show that both have normal interstellar extinction laws in the optical as well as in the near-IR band. From the ultraviolet excess measurement, we derive metallicities of [Fe/H] $= -0.025 \pm 0.01$ dex and -0.042 ± 0.01 dex for the clusters Be 24 and Cz 27, respectively. The distances, as determined from main sequence fitting, are 4.4 ± 0.5 kpc and 5.6 ± 0.2 kpc. The comparison of observed CMDs with $Z = 0.01$ isochrones, leads to an age of 2.0 ± 0.2 Gyr and 0.6 ± 0.1 Gyr for Be 24 and Cz 27, respectively. In addition to this, we have also studied the mass function and dynamical state of these two clusters for the first time using probable cluster members. The mass function is derived after including the corrections for data incompleteness and field star contamination. Our analysis shows that both clusters are now dynamically relaxed.

Key words: astrometry – proper motions – Hertzsprung–Russell and colour–magnitude diagrams – stars: luminosity function, mass function – open clusters and associations: individual: Berkeley 24 and Czernik 27.

1 INTRODUCTION

Galactic clusters contain from a few tens to several thousands stars, which are loosely concentrated and gravitationally bound to each other. Open clusters are important tools for the study of Galactic structure (Janes & Alder 1982), chemical evolution (Magrini et al. 2009) and star formation processes in the Milky Way Galaxy. Galactic clusters offer the advantage of studies of field stars that their

ages and distances can be determined from main sequence fitting (Carraro, Beletsky & Marconi 2013). In particular, the intermediate/old age open clusters are very useful in testing stellar isochrones and dynamical evolution of the stars. Furthermore, they are found in all parts of Milky Way galaxy and exhibit very wide range in their ages. A new era in dynamical astronomy has begun with the second data release of the Gaia (GDR2) mission in 2018 April (Brown et al. 2018).

The distribution of stellar masses that results from a star formation event is called the initial mass function (IMF). The IMF is the key parameter for constraining star formation theories and also to understand the subsequent stellar evolution process. In

★ E-mail: devendrabisht297@gmail.com (DB); arerkant@aries.res.in, (RKSY); shashi@prl.res.in (SG)

Table 1. Fundamental parameters of the clusters Be 24 and Cz 27 are taken from Dias et al. (2002) and WEBDA.

Name	α_{2000} h:m:s	δ_{2000} d:m:s	l (deg)	b (deg)	Dia (′)	$E(B-V)$ (mag)	D (pc)	Log(age)
Be 24	06:37:47	−00:52:19	210.6	−2.6	7	0.4	4700	9.34
Cz 27	07:03:22	6:23:47	208.5	5.5	5	0.15	5800	8.80

the recent years, the mass function has been determined for a number of open clusters by numerous authors (e.g. Hur, Sung & Bessell 2012; Melnikov & Eisl'offel 2012; Khalaj & Baumgardt 2013). It is still not well understood if the shape of the IMF is universal in time and space or if it depends upon astrophysical parameters like metallicity, cluster extent, etc. (e.g. Scalo 1986, 1998).

Open clusters are very important objects for the investigation of the dynamical evolution of stellar system, because the stars in clusters are born from the same molecular cloud and have evolved in the same gravitational potential. Energy equipartition due to interactions between cluster stars leads to mass segregation. The equipartition of energy takes place after many encounters between the members of a cluster. This causes massive stars to lose kinetic energy and fall towards the cluster centre, while lower mass stars increase their velocity and move outwards. The encounters continue until the system becomes relaxed. The relaxation time-scale depends on the number of stars in a cluster (Bonnell & Davies, 1998). Mass segregation results in a steeper mass function slope in the outer region of the cluster (Ann & Lee 2002). The process also causes some fraction of the low-mass stars to evaporate from the cluster to create a halo of predominantly low-mass stars surrounding the cluster (Eggen 1993).

In this study, we consider two open clusters, Berkeley 24 and Czernik 27 (Be 24 and Cz 27 in the following), which are situated between Perseus and the outer arm in the third Galactic quadrant of the Milky Way. The basic parameters available in the literature (Dias et al. 2002) are provided in Table 1. Here, we list what has been published on these clusters in the literature:

Be 24: Ortolani, Bica & Barbuy (2005) studied this cluster using *BV* photometry and estimated the reddening and distance to be $E(B-V) = 0.40$ mag and 4.7 kpc, respectively.

Cz 27: This is a relatively faint cluster recognized in Monoceros by Czernik (1966). Kim et al. (2005) found that Cz 27 is a moderately reddened ($E(B-V) = 0.15$) cluster with an age similar to the Hyades located 5.8 kpc from the Sun. Cz 27 was later studied by Piatti, Claria & Ahumada (2010) using $UBVI_{KC}$ photometry and they found that this is an intermediate age star cluster. They derived the reddening to be $E(B-V) = 0.08$ mag, and inferred a significantly smaller distance of 2.1 kpc and an age of about 0.7 Gyr.

From the previous studies, we can see that there is some disagreement in the basic parameters of the clusters between different studies. Hence, a detailed study of these objects is justified to try to clarify these disagreements. In addition to this, these clusters make a bridge between young open clusters and globular clusters in understanding the dynamical evolution of clusters. Therefore, in this article, we provide new *UBVI* CCD photometry of Be 24 and Cz 27, and study their basic parameters along with their mass functions and dynamical evolution.

The plan of this paper is as follows. We describe our observations and data reduction techniques in Section 2. Sections 3 and 4 deal with the derivation of the basic parameters of the clusters. Section 5 is devoted to the luminosity and mass function of the clusters. The

Table 2. Log of observations, with dates and exposure times for each passband.

Band	Exposure time (in seconds)	Date
	Be 24	
U	$1500 \times 2, 300 \times 1$	2010 Dec 5
B	$1200 \times 2, 240 \times 2$	,,
V	$900 \times 3, 120 \times 1$	,,
I	$300 \times 2, 120 \times 2$	,,
	Cz 27	
U	$1500 \times 2, 300 \times 1$	2010 Nov 7
B	$1200 \times 2, 240 \times 2$	,,
V	$900 \times 2, 180 \times 2$	,,
I	$300 \times 2, 120 \times 1$	,,

dynamical state of the clusters is described in Section 6. Finally, we summarize our results in the last section.

2 OBSERVATIONS AND DATA REDUCTION

We have used CCD imaging to obtain new *UBVI* photometry of stars in the region of our two clusters of interest, Be 24 and Cz 27. These data were obtained using the 104-cm Sampurnanand Reflector Telescope (f/13) located at Aryabhatta Research Institute of Observational Sciences, Manora Peak, Nainital, India. Images were acquired using a 2K × 2K CCD, which has 24 μm square pixels, resulting in a scale of 0″.36 pixel^{-1} and a square field of view of 12′.6 size. The CCD gain was 10 e$^-$/ADU while the read out noise was 5.3 e$^-$. In order to improve the S/N ratio, the observations were taken in the 2 × 2 pixel^2 binned mode. The observations were organized in several short exposures in each of the filters as specified in Table 2. In Table 2, we also list the observing dates. The identification maps based on our *V*-band observations are shown in Fig. 1.

To clean the science images, a number of bias and twilight flat-field frames were taken in *V*, *B*, *I*, and *U*, during the two observing nights. The IRAF[1] data reduction package was used for initial processing of data frames which includes bias subtraction, flat-fielding, and cosmic ray removal. Stellar magnitudes were obtained by using the DAOPHOT software. The instrumental magnitudes were derived through point spread function (PSF) fitting using DAOPHOT/ALLSTAR (Stetson 1987, 1992) package. To determine the PSF, we used several well-isolated stars distributed over the entire frame. The Gaussian function was used as an analytical model PSF. The shape of the PSF was made to vary quadratically with position on the frame. Appropriate aperture corrections were calculated using isolated and unsaturated bright stars in the frame.

---

[1] IRAF is distributed by the National Optical Astronomical Observatory which are operated by the Association of Universities for Research in Astronomy, under contract with the National Science Foundation.
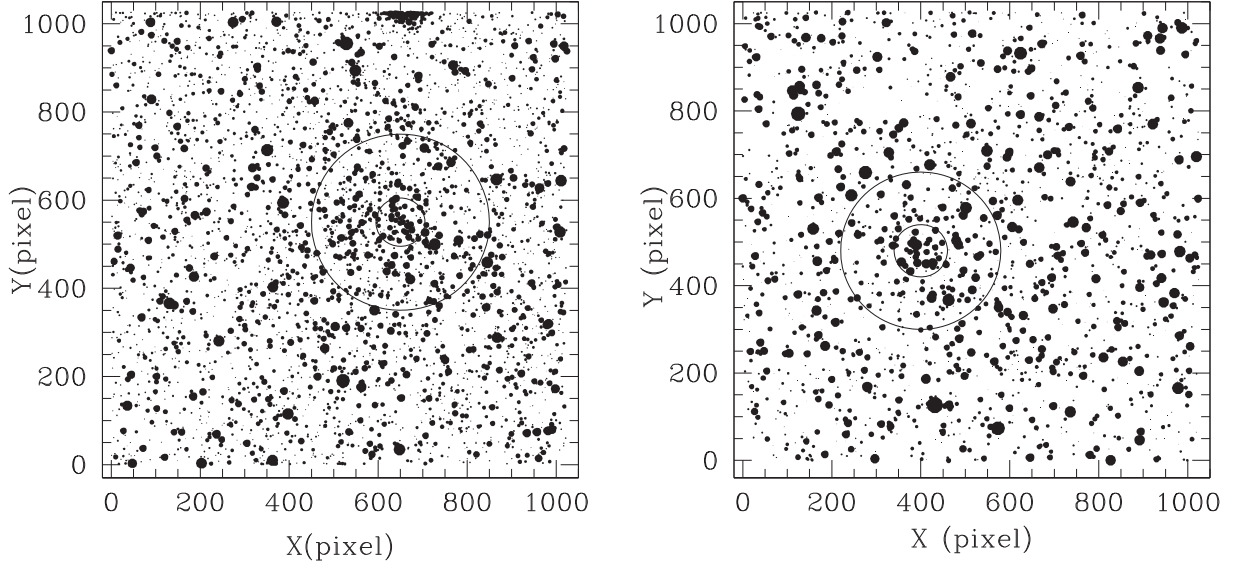
Figure 1. Finding chart of the stars in the field of Be 24 and Cz 27. Filled circles of different sizes represent brightness of the stars. Smallest size denotes stars of $V \sim 20$ mag. Open outer circle represent the cluster size and inner circle represent core region.

ALLSTAR computes x and y centres, sky values, and magnitudes for the stars by fitting the PSF to groups of stars in the image. Initial estimates of the centres, sky values, and magnitudes are read from the aperture photometry file. ALLSTAR groups the stars dynamically, performing a regrouping operation after every iteration. The new computed centres, sky values, and magnitudes are written in a file along with the number of iterations it took to fit the star, the goodness of fit (chi) and sharpness. An image with all the fitted stars subtracted out is written in another image. In effect, ALLSTAR performs the combined operations of GROUP, NSTAR, and SUBSTAR from DAOPHOT.

We have cross-identified the stars of different frames and filters using the DAOMATCH/DAOMASTER programme available in daophot II. To determine the transformation coefficients from instrumental to standard magnitudes, the CCDLIB and CCDSTD routines were used. Finally, standard magnitudes and colours of all the stars were obtained using the routine FINAL.

2.1 Photometric calibration

We observed the standard field SA 98 (Landolt 1992) during both observing nights for the purpose of photometric calibration of the CCD system. The standard stars used in the calibrations have brightness and colour range $12.77 \leq V \leq 16.11$ and $-0.329 < (B-V) < 1.448$, respectively, thus covering the range relevant for the bulk of the cluster stars. For the atmospheric extinction coefficients, we assumed the typical values for the ARIES site (Kumar et al. 2000). For translating the instrumental magnitude to the standard magnitude, the calibration equations derived using least square linear regression are as follows:

$$u = U + Z_U + C_U(U - B) + k_U X$$
$$b = B + Z_B + C_B(B - V) + k_B X$$
$$v = V + Z_V + C_V(B - V) + k_V X$$
$$i = I + Z_I + C_I(V - I) + k_I X,$$

Table 3. Derived standardization coefficients and their errors.

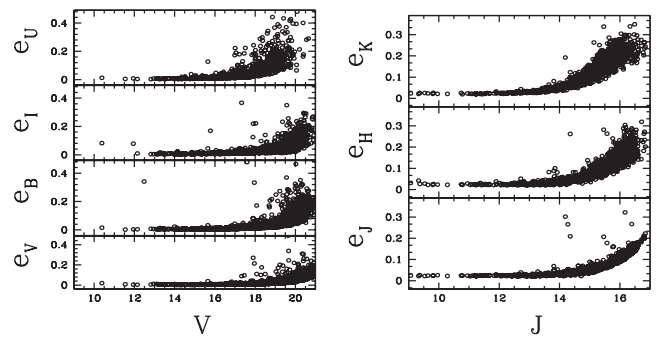| Filter	Colour coeff. (C)	Zeropoint (Z)
	Be 24	
U	-0.040 ± 0.09	7.35 ± 0.05
B	$+0.001 \pm 0.01$	5.29 ± 0.01
V	-0.104 ± 0.01	4.99 ± 0.01
I	-0.125 ± 0.01	5.43 ± 0.01
	Cz 27	
U	-0.03 ± 0.02	7.85 ± 0.01
B	-0.03 ± 0.01	5.64 ± 0.01
V	-0.06 ± 0.01	5.21 ± 0.01
I	-0.06 ± 0.01	5.48 ± 0.01

Figure 2. Photometric errors in different bands against V magnitude (left) and J magnitude (right).

where u, b, v, and i are the aperture instrumental magnitudes, U, B, V, and I are the standard magnitudes, and X is the airmass. The colour coefficients (C) and zeropoints (Z) for the different filters are listed in Table 3. The errors in zero-points and colour coefficients are ~ 0.01 mag except in the U filter where it is 0.09 mag. The internal errors derived from DAOPHOT are plotted against V magnitude in Fig. 2. This figure shows that the average photometric error is ≤ 0.01 mag for B, V, and I filters at $V \sim 19^{th}$ mag, while

Table 4. The rms global photometric errors as a function of *V* magnitude.

V	σ_V	σ_B	σ_I	σ_U
10 − 11	0.05	0.05	0.05	0.05
11 − 12	0.05	0.05	0.03	0.05
12 − 13	0.05	0.05	0.05	0.06
13 − 14	0.05	0.05	0.05	0.06
14 − 15	0.05	0.05	0.05	0.06
15 − 16	0.05	0.05	0.05	0.08
16 − 17	0.05	0.05	0.05	0.11
17 − 18	0.06	0.06	0.06	0.13
18 − 19	0.06	0.06	0.06	0.20
19 − 20	0.07	0.08	0.07	0.31

it is ≤ 0.03 mag for *U* filter at $V \sim 18^{th}$ mag. Global photometric (DAOPHOT + Calibrations) errors are also calculated and listed in Table 4. For the *V* filter, the errors are 0.05 at $V \sim 17$ mag and 0.07 at $V \sim 20$ mag. The final photometric data are available in electronic form at the WEBDA site[2] and also upon request directly from the authors.

In order to transform CCD pixel coordinates to celestial coordinates, we have used the online digitized European Southern Observatory catalogue included in the SKYCAT software as an absolute astrometric reference frame. The *CCMAP* and *CCTRAN* routines in IRAF were used to find a transformation equation which gives the celestial coordinates as a function of the pixel coordinates. The resulting celestial coordinates have a standard deviation of 0.1 arcsec in both right ascension and declination.

2.2 The 2*MASS* data

The near-Infrared JHK_s photometric data for clusters Be 24 and Cz 27 were taken from the *Two Micron All-Sky Survey* (2*MASS*). 2*MASS* uniformly scanned the entire sky in three near-IR bands $J(1.25\mu m)$, $H(1.65\mu m)$, and $K_s(2.17\mu m)$. The 2*MASS* (Skrutskie et al. 2006) used two highly automated 1.3m aperture, open tube, equatorial fork-mount telescopes [one at Mt. Hopkins, Arizona (AZ), USA and other at CTIO, Chile] with a 3-channel camera (256 × 256) array of HgCdTe detectors in each channel). The 2*MASS* data base provides photometry in the near-infrared *J*, *H*, and K_s bands to a limiting magnitude of 15.8, 15.1, and 14.3, respectively, with a signal-to-noise ratio (S/N) greater than 10. We retain only those sources for which the error in each band is less than 0.15 mag to ensure a sufficient photometric accuracy. The errors given in the 2*MASS* catalogue for the *J*, *H*, and K_s bands are plotted against *J* magnitudes in Fig. 2. This figure shows that the mean errors in the *J*, *H*, and K_s bands are all ≤ 0.05 mag at $J \sim 13$ mag. The errors become ~ 0.1 mag at $J \sim 15$ mag.

2.3 Gaia DR2

We used GDR2 (Brown et al. 2018) for proper motion study of clusters Be 24 and Cz 27. This data contains five parametric astrometric solution-positions on the sky (α, δ), parallaxes and ($\mu_\alpha \cos\delta$, μ_δ) with a limiting magnitude of $G = 21$ mag. Parallax uncertainties are in the range of up to 0.04 mas for sources at $G \leq 15$ mag, around 0.1 mas for sources with $G \sim 17$ mag. The uncertainties in the
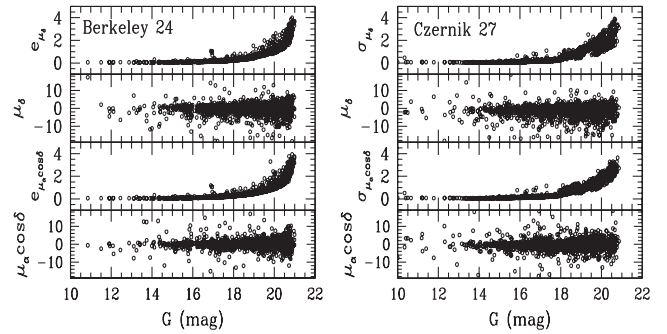
Figure 3. Plot of proper motions and their errors versus *G* magnitude.
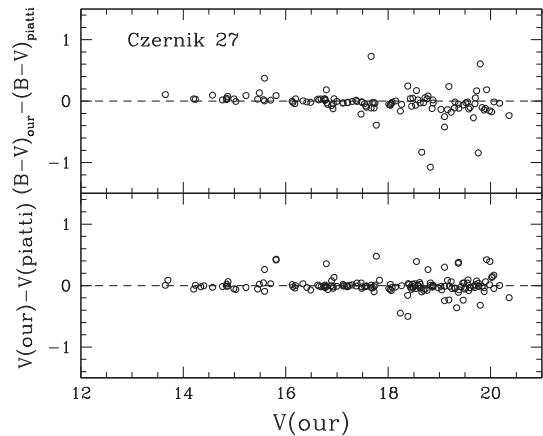
Figure 4. Differences between measurements presented in Piatti et al. (2010) and in this study for *V* magnitude and $(B - V)$ colours. Zero difference is indicated by the dashed line.

respective proper motion components are up to 0.06 mas yr^{-1} (for $G \leq 15$ mag), 0.2 mas yr^{-1} (for $G \sim 17$ mag), and 1.2 mas yr^{-1} (for $G \sim 20$ mag). The proper motion and their corresponding errors are plotted against *G* magnitude as shown in Fig. 3 for clusters Be 24 and Cz 27. In this figure, errors in proper motion components are ~ 1.2 at $G \sim 20$ mag.

2.4 Comparison with previous photometry

The *CCD UBVI$_{KC}$* photometry down to $V \sim 21.0$ for the open cluster Cz 27 has been discussed by Piatti et al. (2010). We have cross-identified stars in the two catalogues on the assumption that stars are correctly matched if the difference in position is less than 1 arcsec. On this basis, we have found 154 common stars. A comparison of *V* magnitudes and $(B - V)$ colours between the two catalogues is shown in Fig. 4. The mean difference and standard deviation per magnitude bin are given in Table 5. This indicates that our *V* and $(B - V)$ measurements are in fair agreement with those given in Piatti et al. (2010). For Be 24, there is no photometric catalogues available in the literature. Our deep photometry for this cluster is the first publicly available catalogue.

3 MEAN PROPER MOTION OF THE CLUSTERS

To derive the mean proper motion of the clusters, *GDR*2 data are used for both the clusters. In this catalogue, we can find the mean positions and proper motions for all objects down to $G \sim 20$ mag.

Table 5. Differences in V and $(B - V)$ between Piatti et al. (2010) and our study. The standard deviation in the difference for each magnitude bin is also given in the parentheses.

V	ΔV	$\Delta(B - V)$
$13 - 14$	$-0.02\sim(0.03)$	$0.02\sim(0.04)$
$14 - 15$	$-0.07\sim(0.05)$	$0.03\sim(0.03)$
$15 - 16$	$0.06\sim(0.20)$	$0.01\sim(0.12)$
$16 - 17$	$-0.06\sim(0.08)$	$-0.09\sim(0.18)$
$17 - 18$	$-0.05\sim(0.10)$	$-0.07\sim(0.26)$
$18 - 19$	$-0.09\sim(0.14)$	$-0.04\sim(0.18)$
$19 - 20$	$-0.04\sim(0.19)$	$-0.11\sim(0.25)$

The mean proper motion is defined as the average angular speed of cluster per year by which it has changed its position over the sky. PMs $\mu_\alpha cos\delta$ and $\mu\delta$ are plotted as VPDs in the bottom panels of Fig. 5. The top panels shows corresponding V versus $(B - V)$ CMDs. The left-hand panel show all stars, while the middle and right-hand panels show the probable cluster members and field stars. A circle of 0.6 and 1 mas yr^{-1} around the cluster centre for Be 24 and Cz 27, respectively, in the VPD defines our membership criteria. The chosen radius is a compromise between loosing cluster members with poor PMs and including field region stars. The CMD of the probable cluster members are shown in the upper-middle panels in Fig. 5. The main sequence of the clusters are clearly separated out. These stars have a PM error of $\leq 1\sim$mas yr^{-1}.

To determine the mean proper motion of the clusters, we considered probable cluster members based on VPD and CMD for clusters Be 24 and Cz 27, respectively, as shown in Fig. 5. We have constructed the histograms and fitted the Gaussian function to the central bin, which provides mean proper motion in both directions as shown in Fig. 6. We have thus found the mean-proper motion of Be 24 as 0.35 ± 0.06 mas yr^{-1} and 1.20 ± 0.08 mas yr^{-1} in RA and DEC directions, respectively, while the same for cluster Cz 27 are found to be -0.52 ± 0.05 mas yr^{-1} and -1.30 ± 0.05 mas yr^{-1}. The mean proper motion of the clusters is determined as follows:

$$\mu = \sqrt{\left(\mu_x^2 + \mu_y^2\right)}.$$

The estimated value of mean proper motion is found to be 1.25 ± 0.09 mas yr^{-1} and 1.40 ± 0.05 mas yr^{-1} for the clusters Be 24 and Cz 27, respectively. Here, the uncertainties are standard deviations.

4 STRUCTURAL PARAMETERS, COLOUR–MAGNITUDE DIAGRAMS, REDDENING LAW AND METALLICITY OF THE CLUSTERS

4.1 Centre estimation

To study the shape of a star cluster, the first necessary step is to identify the cluster centre. The location of maximum stellar density of the cluster's area is defined as the cluster centre. Earlier studies have estimated cluster centres by visual inspection (e.g. Becker & Fenkart 1971; Romanishim & Angel 1980), but in this analysis, we have applied the star-count method to the observed area of each cluster. To estimate the cluster centre, we have plotted the histogram of star counts in Right Ascension (RA) and Declination (DEC) of the stars using GDR2. For this purpose, the cluster area is divided into equal sized bin in RA and DEC. The purpose of

this counting process is to estimate the maximum central density of clusters. The cluster centre is determined by fitting Gaussian profiles of star counts in RA and DEC, as shown in Fig. 7. The best-fitting Gaussian profiles provide the central coordinates of the clusters as $\alpha = 99.45 \pm 0.004$ deg and $\delta = -0.87 \pm 0.003$ deg for Be 24 and $\alpha = 105.81 \pm 0.007$ deg and $\delta = 6.41 \pm 0.005$ deg for Cz 27. These fitted values of the cluster centres are in very good agreement with the values listed from the literature in Table 1. We have adopted these fitted centres for further analysis.

4.2 Size of the clusters

Determination of the cluster extent is necessary for reliable estimation of all relevant fundamental parameters of open clusters. For this purpose, we have derived the surface stellar density by performing star counts in concentric rings around our fitted centres of the clusters, and then divided by their respective areas. In Fig. 8, we have shown the density profile (log(radius) versus log(density)) for both the clusters. This density distribution shows a peak near the cluster centre and becomes consistent with being flat after a certain point where the cluster density merges into the field star density. Therefore, we have considered 2.7(log(radius) = 0.43) and 2.3 (log(radius) = 0.36) arcmin as the cluster radius for Be 24 and Cz 27, corresponding to 3.4 and 3.2 pc, respectively. A smooth continuous line representing a King (1962) profile:

$$f(r) = f_{\text{bg}} + \frac{f_0}{1 + (r/r_c)^2}$$

has been fitted to the radial density profiles. Here, r_c, f_0, and f_{bg} are the core radius, central density, and the background density, respectively. The core radius is defined as a distance where the stellar density becomes half of the central density. By fitting the King model to the radial density profile, we found core radii as 0.5 (log(core radius) = -0.30) and 0.47 (log(core radius) = -0.32) arcmin as shown in Fig. 8 for Be 24 and Cz 27, respectively. The estimated values of core radii along with the other structural parameters are listed in Table 6 for both the clusters. The location of cluster radii and core radii indicated by arrow in the radial density profiles. The cluster limiting radius, r_{lim}, was calculated by comparing $f(r)$ to a background density level, f_b, defined as:

$$f_b = f_{\text{bg}} + 3\sigma_{\text{bg}},$$

where σ_{bg} is uncertainty of f_{bg}. Therefore, r_{lim} was calculated according to the following formula

$$r_{\text{lim}} = r_c \sqrt{\left(\frac{f_0}{3\sigma_{\text{bg}}} - 1\right)}.$$

The value for the limiting radius was found to be 3.0 and 3.8 arcmin for Be 24 and Cz 27, respectively. r_c and r_{lim} can be combined to calculate the concentration parameter $c = \log(\frac{r_{\text{lim}}}{r_c})$ (Peterson & King, 1975) to further characterize the structure of clusters in the Milky Way Galaxy. In this study, we found the concentration parameters to be 0.7 for both clusters. Maciejewski & Niedzielski (2007) reported that r_{lim} may vary for individual clusters from $2r_c$ to $7r_c$. In this case, both clusters show good agreement with Maciejewski & Niedzielski (2007).

The density contrast parameter is estimated for clusters using the following relationship
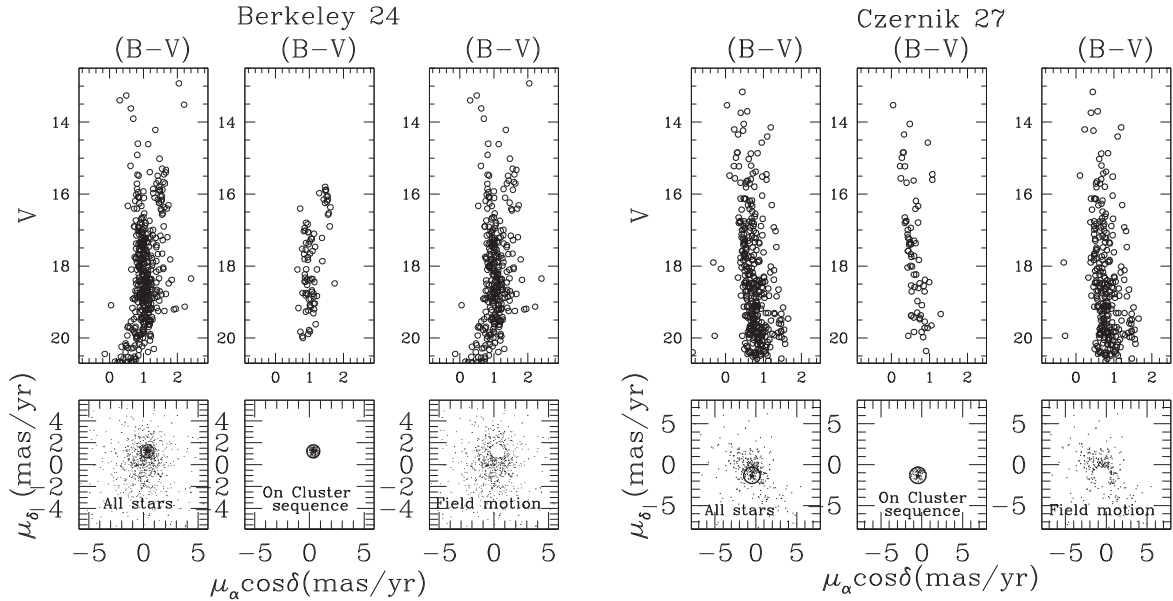
$$\delta_c = 1 + \frac{f_0}{f_{\text{bg}}}.$$

Figure 5. (Bottom panels) Proper-motion vector point diagram (VPD) for Be 24 and Cz 27. (Top panels) V versus $(B - V)$ colour–magnitude diagrams (CMDs). (Left) The entire sample. (Centre) Stars in VPDs within circle of 0.6 mas yr^{-1} and 1 mas yr^{-1} for Be 24 and Cz 27, respectively, of the cluster mean. (Right) Probable background/foreground field stars in the direction of these clusters. All plots show only stars with PM σ smaller than 1 mas yr^{-1} in each coordinate.
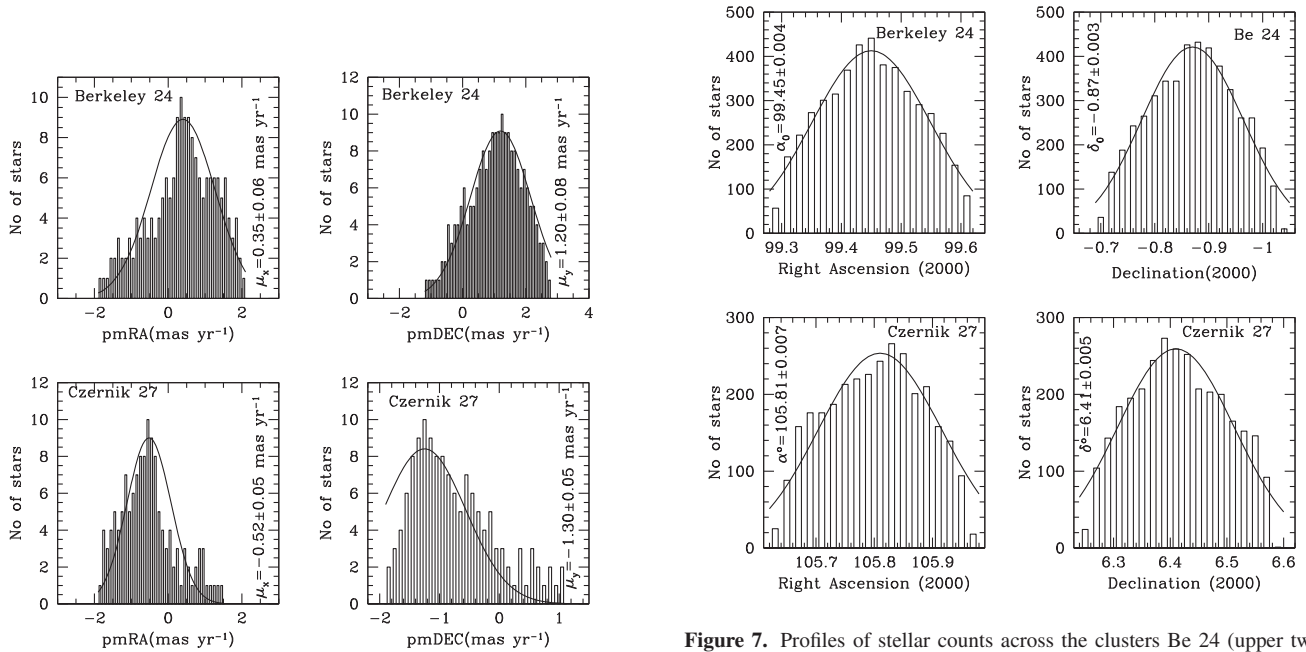

Figure 6. Proper motion histograms of 0.1 mas yr^{-1} bins in right ascension and declination of the candidate clusters. The Gaussian function fit to the central bins provides the mean values in both directions as shown in each panel.

Figure 7. Profiles of stellar counts across the clusters Be 24 (upper two panels) and Cz 27 (lower two panels). Gaussian fits have been applied to derive the centroid of the two clusters in right ascension and declination.

We found values of δ_c of 6.7 and 6.0 for Be 24 and Cz 27, respectively. These values of δ_c are lower than the values ($7 \le \delta_c \le 23$) derived for compact star clusters by Bonatto & Bica (2009). This implies that both clusters studied here are sparse clusters.

The tidal radius of open clusters is the distance from the cluster core at which the gravitational influence of the Galaxy is equal to
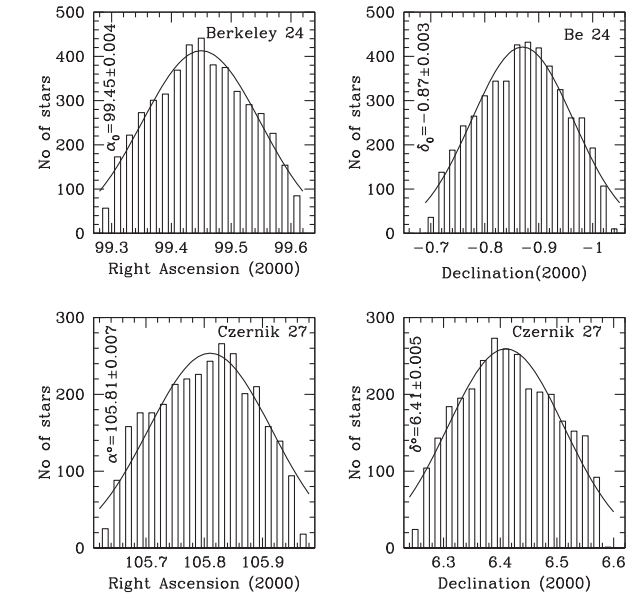
that of the open cluster core. The tidal radius of a cluster can be estimated using the following procedure.

The Galactic mass M_G inside a Galactocentric radius R_G is given by (Genzel & Townes, 1987)

$$M_G = 2 \times 10^8 \, \mathrm{M_\odot} \left(\frac{R_G}{30 \, \mathrm{pc}} \right)^{1.2}.$$

The value of M_G is found to be $2.8 \times 10^{11} \, \mathrm{M_\odot}$ and $3.2 \times 10^{11} \, \mathrm{M_\odot}$ for clusters Be 24 and Cz 27, respectively.
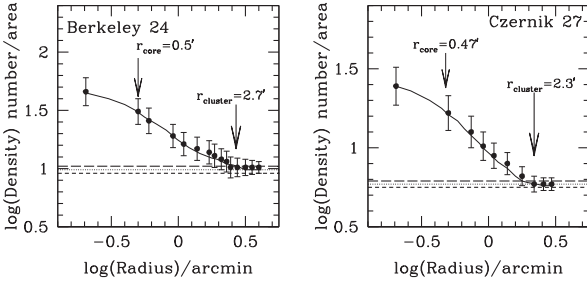
Figure 8. Surface density distribution of the clusters Be 24 and Cz 27. Errors are determined from sampling statistics (= $\frac{1}{\sqrt{N}}$ where N is the number of stars used in the density estimation at that point). The smooth line represent the fitted profile whereas dotted line shows the background density level. Long and short dashed lines represent the errors in background density. Arrow indicates the location of cluster and core radii.

Using the formula by Kim et al. (2000), tidal radius R_t of a cluster is,

$$R_t = \left(\frac{M_c}{2M_G} \right)^{1/3} \times R_G,$$

where R_t and M_c are the tidal radii and total mass (see Section 8) of the clusters, respectively. We derive values of the tidal radius of 6.7 and 6.3 pc for Be 24 and Cz 27, respectively. These are also listed in Table 6. Our measurement is reliable because it is based on the probable members of the clusters selected from VPD.

4.3 Reddening law

The plots of TCDs for various sets of two colours are very useful tools to estimate interstellar reddening and to understand the properties of the extinction law in the direction of the clusters.

4.3.1 Total-to-selective extinction value

Reddening is an important basic parameter of a star cluster, since it can significantly affect the determination of other fundamental parameters. To derive the characteristics of the extinction law, it is important to analyse TCDs. The emitted photons of cluster stars are scattered and absorbed in the interstellar medium by dust particles, which leads to deviation of colours from their intrinsic values. The normal Galactic reddening law is often not applicable in the line of sight to clusters (e.g. Sneden et al. 1978). Chini & Wargue (1990) suggested $(V - \lambda)/(B - V)$ TCDs to examine the nature of the reddening law. Here, λ denotes nearly any filter other than V. We have studied the reddening law for both clusters by drawing TCDs as shown in Fig. 9. Since the stellar colour values are found to be linearly dependent on each other, then a linear equation is applied to calculate the slope ($m_{cluster}$) of each TCD. We have estimated total-to-selective extinction using the relation given by Neckel & Chini (1981):

$$R_{cluster} = \frac{m_{cluster}}{m_{normal}} \times R_{normal},$$

where $m_{cluster}$ is the typical value of the slope in a TCD and R_{normal} (numerically 3.1) is the normal value of total to selective extinction ratio. We have estimated $R_{cluster}$ in different passbands to be $3.1 \leq R_{cluster} \leq 3.5$, which is slightly larger than the normal value. Thus, reddening law is found to be normal towards the cluster region for both clusters.

4.3.2 (U − B) versus (B − V) diagram

A knowledge of reddening is very important for the intrinsic properties of cluster stars. In the absence of spectroscopic data, the $(B - V)$, $(U - B)$ colour–colour diagram is widely used for the reddening estimation (e.g. Becker & Stock 1954). To estimate the reddening towards the cluster region, we have plotted $(U - B)$ versus $(B - V)$ diagram for both the clusters as shown in Fig. 10 using stars within cluster extent. The intrinsic zero-age main-sequence (ZAMS) given by Schmidt-Kaler (1982) is fitted by the continuous curve assuming the slope of reddening $E(U - B)/E(B - V)$ as 0.72. By fitting ZAMS to the MS, we have calculated mean value of $E(B - V) = 0.45 \pm 0.05$ mag for Be 24 and $E(B - V) = 0.15 \pm 0.05$ for Cz 27, respectively. Our derived values of reddening agree fairly well with the values estimated by others as discussed in Section 1.

4.3.3 Interstellar extinction in near-IR

2MASS JHKs data combined with optical data is used to study the interstellar extinction law towards the cluster region. The K_s magnitude is converted into K magnitude using the formulations by Persson et al. (1998). The $(J - K)$ versus $(V - K)$ diagram for both the clusters are shown in Fig. 11. The ZAMS is taken from Caldwell et al. (1993) for $Z = 0.01$ is shown by a solid line. The fit of ZAMS provides $E(J - K) = 0.23 \pm 0.03$ mag and $E(V - K) = 1.23 \pm 0.02$ mag for Be 24 and $E(J - K) = 0.06 \pm 0.02$ mag and $E(V - K) = 0.33 \pm 0.01$ mag for Cz 27. The ratios $\frac{E(J-K)}{E(V-K)} \sim 0.18 \pm 0.06$ for Be 24 and Cz 27 are in good agreement with the normal interstellar extinction value of 0.19 given by Cardelli, Clayton & Mathis (1989). The scatter is primarily due to large error in the *JHK* data.

4.3.4 (B − V) versus (J − K) diagram

We have plotted $(B - V)$ versus $(J - K)$ colour–colour diagram for clusters Be 24 and Cz 27, as shown in Fig. 12. To know the relationship between these two colours, we have used the theoretical isochrones given by Girardi et al. (2000). The colour excess $E(B - V)$ and $E(J - K)$ for Be 24 is found to be 0.45 and 0.23 mag, respectively, whereas for Cz 27 we find 0.15 and 0.08 mag. We got the ratio, $\frac{E(J-K)}{E(B-V)} \sim 0.53$ for both the clusters. In the literature, the above value is mentioned as 0.56, which is computed by using the following relations, $A_k = 0.618 \times E(J - K)$ (Mathis 1990); $A_k = 0.122 \times A_v$ (Cardelli et al. 1989) and $A_v = 3.1 \times E(B - V)$. Our estimated value is in good agreement with the literature.

4.3.5 (J − H) versus (J − K) diagram

$(J - H)$ versus $(J - K)$ colour–colour diagram for clusters Be 24 and Cz 27 is shown in Fig. 13. Stars plotted in this figure are within the cluster extent. The isochrone shown by the solid line is taken from Girardi et al. (2000). From this figure, we have found $E(J - H) = 0.14 \pm 0.05$ and $E(J - K) = 0.24 \pm 0.02$ for Be 24 and for Cz 27, the above values are 0.05 ± 0.03 and 0.10 ± 0.05. The ratio $\frac{E(J-H)}{E(J-K)} = 0.58 \pm 0.06$ for both the clusters are in good agreement with the normal interstellar extinction value 0.55 as suggested by Cardelli et al. (1989). Scattering is larger due to large errors in J, H, and K magnitudes. We can estimate the reddening, $E(B - V)$ using the following relations:

$$E(J - H) = 0.309 \times E(B - V)$$

Table 6. Structural parameters of the clusters Be 24 and Cz 27. Background and central density are in the unit of stars per arcmin^2. Core radius (r_c) and tidal radius (R_t) are in arcmin and pc.

Name	f_0	f_b	r_c (arcmin)	r_c (parsec)	R_t (arcmin)	R_t (parsec)	δ_c
Be 24	52.3	9.08	0.5	0.64	5.4	6.7	6.7
Cz 27	29.1	5.81	0.47	0.76	3.8	6.3	6.0
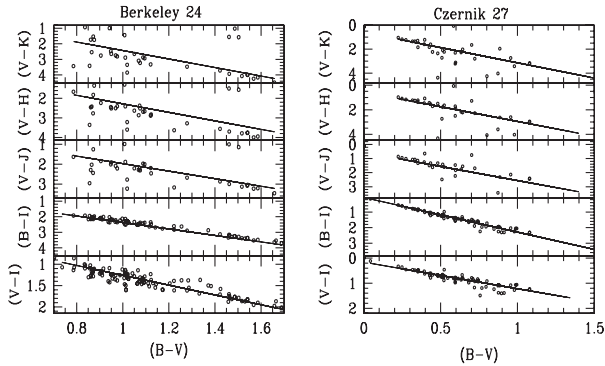
Figure 9. The $(\lambda - V)/(B - V)$ TCD for the stars within cluster extent of clusters Be 24 and Cz 27. The continuous lines represent the slope determined through least-squares linear fit.
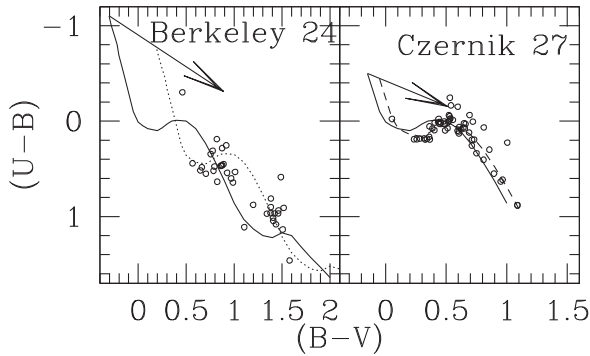
Figure 10. The $(U - B)$ versus $(B - V)$ colour–colour diagram of the clusters. The continuous curve represents locus of Schmidt-Kaler (1982) ZAMS for solar metallicity. Dotted and dashed lines are the shifted Schmidt-Kaler ZAMS with the values given in the text.
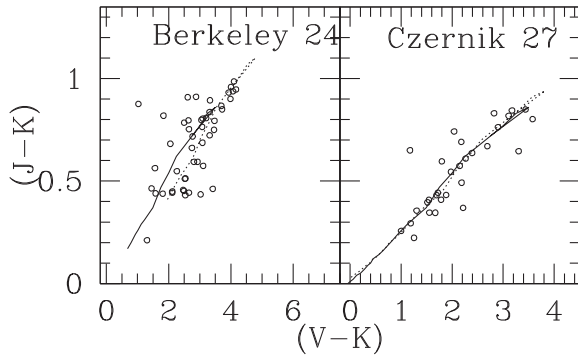
Figure 11. The plot of $(J - K)$ versus $(V - K)$ colour–colour diagram of the clusters for the stars within the cluster radius. Solid line is the ZAMS taken from Caldwell et al. (1993).
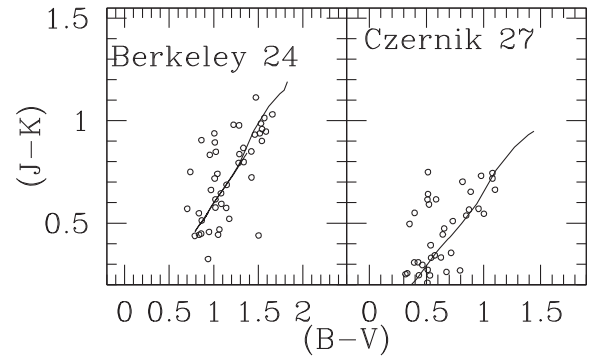

Figure 12. The plot of $(B - V)$ versus $(J - K)$ colour–colour diagram of the clusters for the stars within the cluster radius. Solid line is the theoretical isochrone of Girardi et al. (2000).
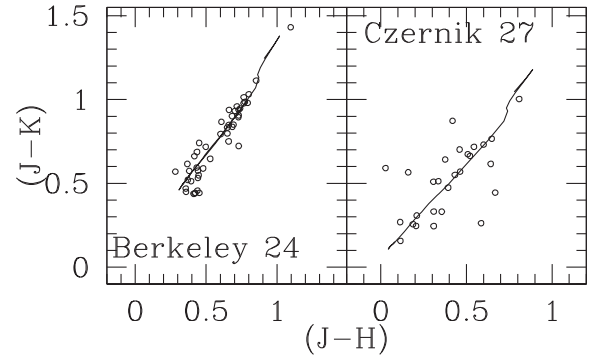

Figure 13. The plot of $(J - H)$ versus $(J - K)$ colour–colour diagram of the clusters for the stars within the cluster radius. Solid line is the theoretical isochrone of Girardi et al. (2000).

$$E(J - K) = 0.48 \times E(B - V).$$

Our estimated values of reddening $E(B - V) = 0.45$ and 0.16 for the cluster Be 24 and Cz 27, using the 2*MASS* colours are similar to those obtained from the $(U - B)$ versus $(B - V)$ colour-colour diagram. Thus, it validates the use of the 2*MASS* colours for the $E(B - V)$ estimation when only 2*MASS* data are available- for e.g. in highly extincted regions.

4.4 Metallicity of the clusters derived from photometry

The metallicity of stars is an important tool to explore the chemical structure and evolution of the Galaxy. The metallicities of the clusters Be 24 and Cz 27 have not been estimated in previous studies. For the estimation of metallicity, we have adopted a method, which is discussed in Karaali et al. (2003), Karaali, Bilir & Tuncel (2005), and Karaali et al. (2011) using *UBV* data. The procedure in this method is based on $F - G$ spectral type main-sequence stars of the
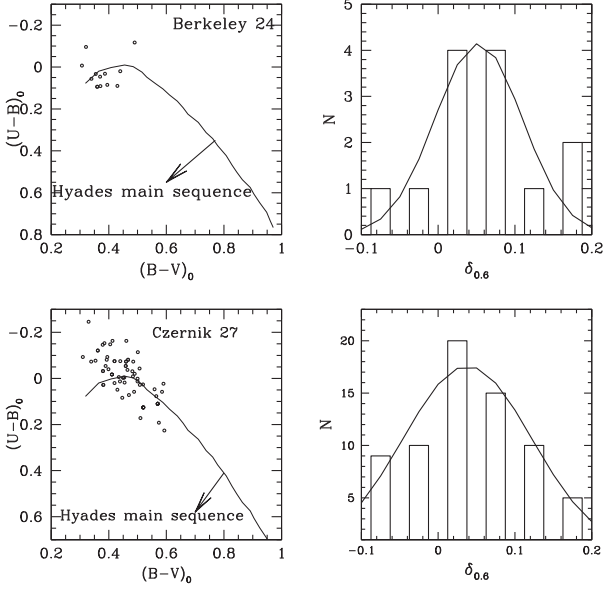
Figure 14. The $(U − B)_0$ versus $(B − V)_0$ TCDs and histograms for the normalized UV-excess for 12 (Be 24) and 69 (Cz 27) main sequence stars used for the metallicity estimation of Be 24 and Cz 27. The solid line in the TCD is Hyades main sequence and solid line in histogram is the Gaussian fit.

cluster. Thus, we selected 69 stars for Cz 27 and 12 stars for Be 24 with colour range $0.3 \leq (B − V)_0 \leq 0.6$ mag consistent with the colours of the $F − G$ spectral types.

We have estimated the normalized ultraviolet (UV) excess for the selected stars, which is defined as the differences between a stars' de-reddened $(U − B)_0$ colour indices and the one corresponding to the members of the Hyades cluster with the same de-reddened $(B − V)_0$ colour index, that is $\delta = (U − B)_{0, H} − (U − B)_{0, S}$. Here, the subscripts H and S indicate Hyades and stars, respectively. In order to utilize the method described in Karaali et al. (2011), we have determined normalized *UV* excesses of the selected stars as described above and normalized their δ differences to the UV-excess at $(B − V)_0 = 0.6$ mag, i.e. $\delta_{0.6}$. $(U − B)_0$ versus $(B − V)_0$ colour–colour diagram and corresponding histograms of the normalized *UV* excesses ($\delta_{0.6}$) of the selected stars for Be 24 and Cz 27 are presented in Fig. 14. By fitting a Gaussian function to this histogram, we have calculated the normalized UV excess of the cluster as $\delta_{0.6} = 0.051 \pm 0.002$ mag for Be 24 and $\delta_{0.6} = 0.039 \pm 0.002$ mag for Cz 27. Here, the uncertainty is given as the statistical uncertainty of the peak of the Gaussian. Then, we have determined the metallicity ($[Fe/H]$) of the clusters by evaluating this Gaussian peak value in the equation discussed in Karaali et al. (2011):

$$rn[Fe/H] = −14.316(\pm1.919)\delta_{0.6}^2 − 3.557(\pm0.285)\delta_{0.6}$$
$$+ 0.105(\pm0.039).$$

The metallicity corresponding to the peak value for the $\delta_{0.6}$ distribution was calculated as $[Fe/H] = −0.025 \pm 0.01$ dex for Be 24 and $[Fe/H] = −0.042 \pm 0.01$ dex for Cz 27. In order to transform the $[Fe/H]$ metallicity obtained from the photometry to the mass fraction Z, the following relation (Mowlavi et al. (2012)) was used:

$$Z = \frac{0.013}{0.04 + 10^{-[Fe/H]}}.$$

Theoretical isochrones corresponding to the metallicity Z, are selected for further estimation of the astrophysical parameters for the clusters. We have found $Z = 0.01$ to be suitable for the clusters.

5 AGES AND DISTANCES OF THE CLUSTERS

The CMD is the most effective tool for the estimation of fundamental parameters such as age and distance for open star clusters. Identification of the main sequence in the cluster's CMD allows a model dependent mass, radius, and distance for each star to be determined. Since samples of stars in the cluster region on the sky are contaminated by the field star population, it is necessary to distinguish the cluster sequence from field-star contamination for the proper analysis of the CMD. We identified probable cluster members using VPD for both clusters. We have also constructed CMDs for stars in the field region as well. Stars present within circular area in VPD for the clusters Be 24 and Cz 27 are considered as cluster region while stars outside this circular area are considered field region stars. The V, $(U − B)$; V, $(B − V)$ and V, $(V − I)$ CMDs of Be 24 and Cz 27 along with the V, $(V − I)$ CMDs of the corresponding field regions are shown in Fig. 15. The CMD constructed using the stars within cluster radius for Be 24 shows main sequence extending down to $V \sim 20$ mag except in the V, $(U − B)$ CMDs where it is only traced down to $V \sim 18.5$ mag. For the cluster Cz 27, CMDs extends down to $V \sim 20$ mag in $V/(B − V)$ and $V/(V − I)$. In V, $(V − I)$ CMDs, we have selected the cluster members by defining the blue and red envelope around the main sequence, as shown in Fig. 15. A star is considered as contaminant if it lies outside the strip in CMDs. Most of the field stars are separated out from the cluster sequence using VPD and photometric criteria in both the clusters. Selected stars are used in LF/MF studies in the next section.

The fundamental parameters: reddening, metallicity, distance modulus, and age of a cluster can be simultaneously determined by fitting the theoretical stellar isochrones to the observed CMDs. In this case, we have used the reliable traditional methods, as discussed above, for the estimation of reddening and metallicity. In order to estimate distance and age of the clusters simultaneously, we have fitted theoretical isochrones given by Girardi et al. (2000) for the MS with $Z = 0.01$. The $V/(U − B)$, $V/(B − V)$, and $V/(V − I)$ CMDs along with visually fitted isochrones are shown in Fig. 16. The detailed shape and position of the different features in the CMD depend mostly on the age and metallicity of the clusters. There is larger photometric scatter at the fainter end of the CMDs. This could be due to larger errors in the photometry or due to contamination of the CMD by field stars. The $E(B − V)$ values for both the clusters are taken from Section 3.4.2.

Be 24: We superimpose isochrones of different age (log(age)=9.25, 9.30 and 9.35 with $Z = 0.01$ in $V/(U − B)$, $V/(B − V)$, and $V/(V − I)$ CMDs. Using turn-off point, we have found an age of 2 ± 0.2 Gyr. On average, we obtained a distance modulus of $(m − M) = 14.80 \pm 0.2$ mag. The estimated distance modulus provides a heliocentric distance as 4.4 ± 0.5 kpc. The estimated distance for this cluster is higher than the 3.7 kpc derived by Koposov et al. (2008) using 2*MASS JHKs* data, but similar to the value 4.4 kpc listed in Dias et al. (2002). The Galactocentric coordinates are $X_\odot = −0.7$ kpc, $Y_\odot = 12.8$ kpc, and $Z_\odot = −0.2$ kpc. The Z coordinate indicates that this cluster is in the thin Galactic disk. The Galactocentric distance of the cluster was calculated to be 12.8 kpc.

Cz 27: As shown in Fig. 16, we have fitted the theoretical isochrones to $V/(U − B)$, $V/(B − V)$, and $V/(V − I)$ CMDs. These isochrones of different age (log(age) = 8.70, 8.80 and 8.90) and $Z = 0.01$ have been superimposed on the CMDs. We have found
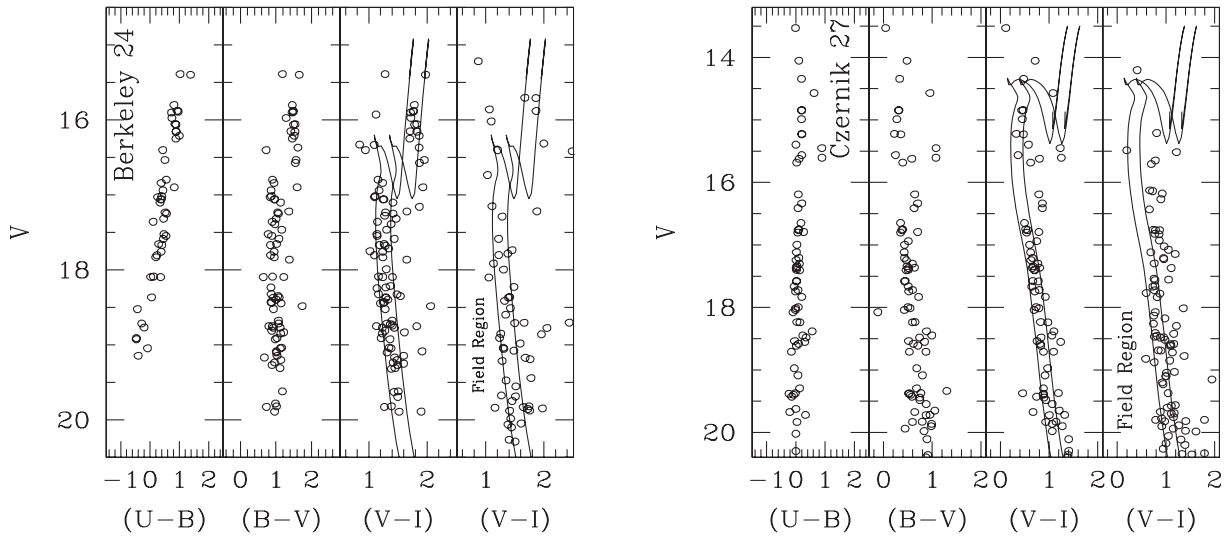
Figure 15. The $V/(U − B)$, $V/(B − V)$, and $V/(V − I)$ CMDs for the clusters Be 24 and Cz 27 using stars within the cluster radius. Stars outside the cluster radius are also plotted as field region stars in $V/(V − I)$ CMD. Solid lines show the blue and red envelope of the MS.
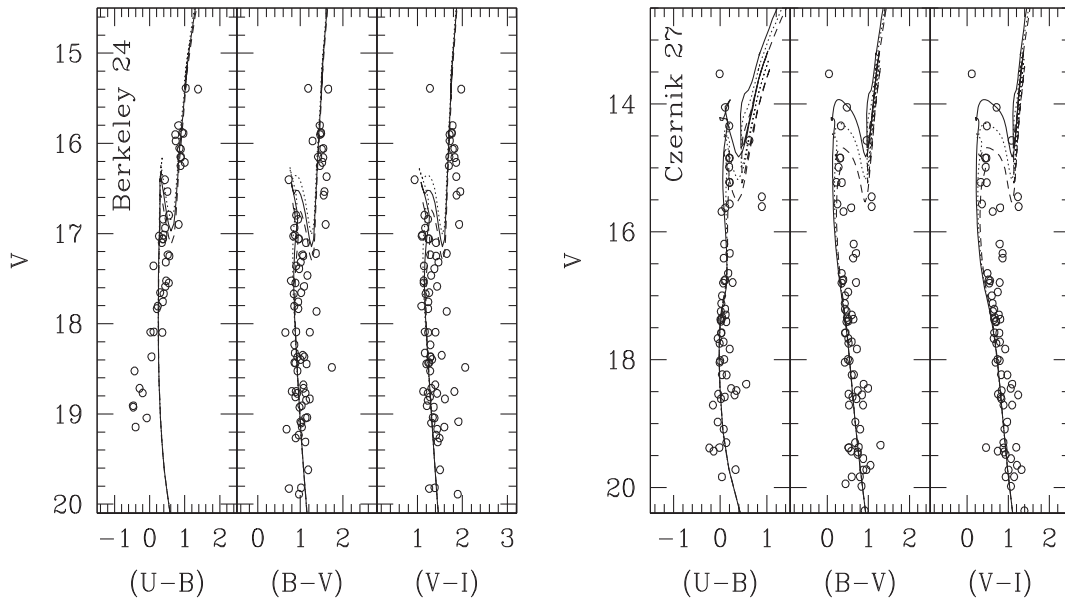
Figure 16. The CMD of the clusters under study. These stars are assumed to be cluster members based on proper motion. The curves are the isochrones of $(\log(\text{age}) = 9.25, 9.30$ and $9.35)$ for the cluster Be 24 and $(\log(\text{age}) = 8.70, 8.80$ and $8.90)$ for the cluster Cz 27. These isochrones are taken from Girardi et al. (2000).

an age of 0.6 ± 0.1 Gyr. The distance modulus $(m − M) = 14.30$ mag provides a heliocentric distance as 5.6 ± 0.2 kpc which is in good agreement with the value 5.8 kpc listed in Dias et al. (2002). The Galactocentric distance is determined as 14.1 kpc, which is determined by assuming 8.5 kpc as the distance of the Sun to the Galactic centre. The Galactocentric coordinates are estimated as $X_\odot = −0.7$ kpc, $Y_\odot = 14.0$ kpc, and $Z_\odot = 0.5$ kpc.

The present age estimated for Be 24 is similar to the age derived by Ortolani et al. (2005) as 2.2 Gyr. For Cz 27, Piatti et al. (2010) estimated an age of 0.7 Gyr, which agrees well within error to the present estimate.

We used parallax of cluster stars taken from GDR2 for both the clusters. We constructed histograms of 0.15 mas bins as shown in Fig. 17 using probable members selected from VPD. Mean parallax
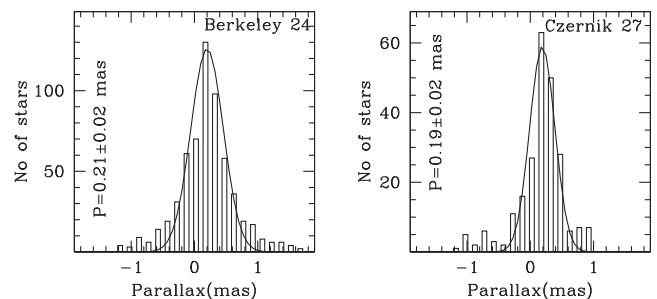
Figure 17. Parallax histograms of 0.15 mas bins for our candidate clusters. The Gaussian function fit to the central bins provides mean parallax.
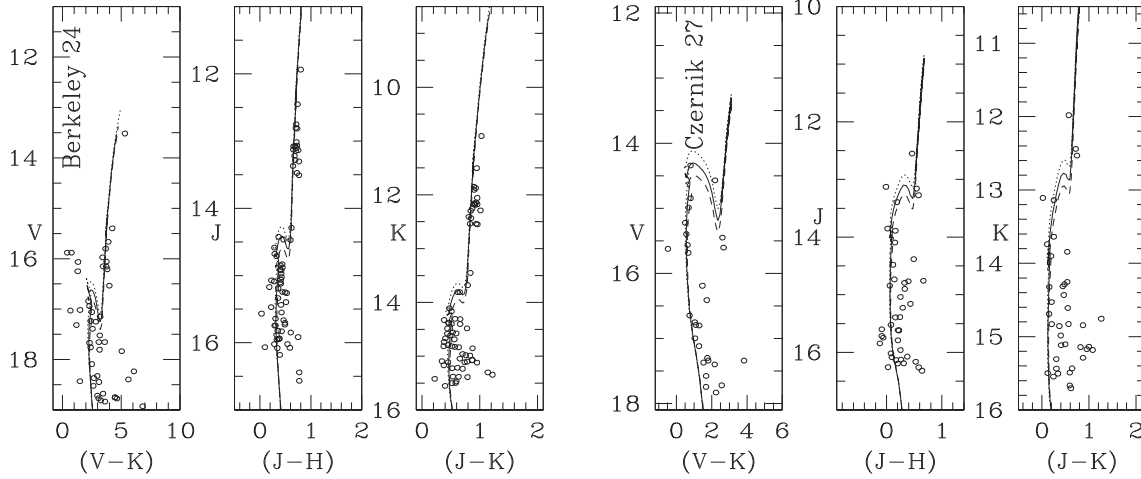
Figure 18. Same as Fig. 16 of optical and near-IR CMDs for Be 24 and Cz 27.

is estimated as 0.21 ± 0.02 mas and 0.19 ± 0.02 mas for clusters Be 24 and Cz 27, respectively, and corresponding distances are 4.7 ± 0.5 kpc and 5.3 ± 0.5 kpc. Estimated values of distance from observed data and from GDR2 are very good in agreement with each other for both clusters.

5.1 Optical and near-IR CMDs

Using both optical and near-IR, data we have re-determined distance and age of the clusters. We have plotted V versus $(V - K)$ and K versus $(J - K)$ CMDs, which is shown in Fig. 18. The theoretical isochrones given by Girardi et al. (2000) for $Z = 0.01$ of $\log(\text{age}) = 9.30$ and 8.80 have been overplotted in the CMDs of Be 24 and Cz 27, respectively. The apparent distance moduli $(m - M)_{V, (V - K)}$ and $(m - M)_{K, (J - K)}$ turn out to be 14.0 ± 0.3 and 12.0 ± 0.3 mag for the cluster Be 24 and 14.0 ± 0.3 and 12.1 ± 0.3 mag for the cluster Cz 27. Using the reddening values estimated in Section 4.3.3, we have derived a distance of 4.3 ± 0.4 kpc for Be 24 and 5.4 ± 0.3 kpc for Cz 27. Both age and distance determination for the clusters are thus in agreement with the estimates using optical data. However, the scatter is larger due to the large errors in the *JHK* magnitudes.

6 LUMINOSITY AND MASS FUNCTION STUDY

To study the luminosity function (LF) and mass function (MF), the first necessary step is to remove the field star contamination from the sample of stars in the cluster region. A statistical field star subtraction method has been used by assuming that the field stars within the cluster and surrounding areas are distributed in a similar way (Wilner & Lada 1991; Phelps & Janes 1993; Sagar & Griffiths 1998). A brief description of the procedure applied here is described in Section 5.

6.1 Completeness of the CCD photometry

Photometric data may be incomplete due to the stellar crowding as well as inefficiency of data reduction programmes. The incompleteness correction is very necessary to compute luminosity function of the stars in the cluster. Completeness corrections were determined by running artificial star experiments on the data. The ADDSTAR routine in DAOPHOT II was used to determine completeness factor (CF). We created several images by adding artificial stars to the

Table 7. Variation of completeness factor (CF) in the $V, (V - I)$ diagram with the MS brightness.

V mag	Be 24			Cz 27		
	Whole	Core	Halo	Whole	Core	Halo
14–15	99.99	99.99	99.99	99.99	99.99	99.99
15–16	99.35	90.90	97.92	99.99	99.99	99.99
16–17	97.56	81.81	97.91	99.65	94.11	95.18
17–18	97.15	93.54	90.56	94.39	88.00	95.04
18–19	94.42	93.11	93.49	88.48	86.95	90.68
19–20	88.97	92.25	92.44	65.94	49.05	72.26

original V image. Stars were added at same geometrical positions in I-band image. Stars found in both V and I band were considered as real detection. In order to avoid appreciable increase in the crowding, we have randomly added only 10 to 15 per cent of actually detected stars of known magnitude and position into the original images. The luminosity distribution of artificial stars is chosen in such a way that large number of stars are inserted into the fainter magnitude bins. This is the range of magnitudes where significant losses due to incompleteness are expected (Bellazzini et al. 2002). Detailed information about this experiment is given by Yadav & Sagar (2002) and Sagar & Griffiths (1998). The added star images are re-reduced using the same method, which was adopted for the original images. The ratio of recovered to added stars in different magnitude bins gives the CF. We have estimated CF in core, halo, and overall region for both the clusters. The CF derived in this way are listed in Table 7 for the clusters Be 24 and Cz 27. As expected, the incompleteness of the data increases with increasing magnitude and increasing stellar crowding. Table 7 shows the value of CF in different magnitude bins and in different regions. The variation of CF versus V magnitude and radius for both the clusters Be 24 and Cz 27 are shown in Fig. 19. The value of CF is $\sim$90 per cent and $\sim$65 per cent at 20 mag in V band for clusters Be 24 and Cz 27, respectively. CF versus radius curve indicates that the CF is more than 75 per cent for both the clusters within cluster extent.

6.2 Luminosity function

We have used the $V/(V - I)$ CMD to construct the luminosity function (LF) for target clusters. In $V/(V - I)$ diagram, we used
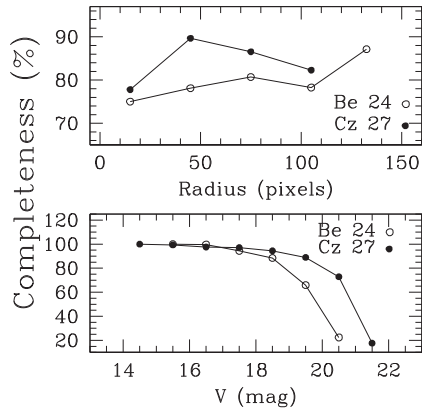
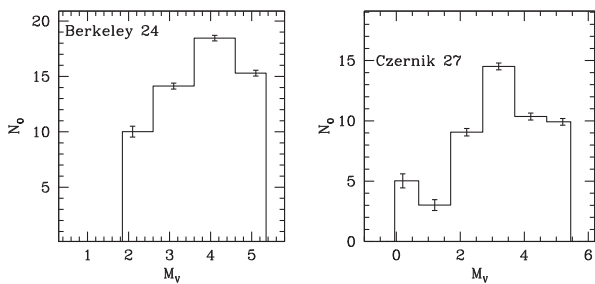**Figure 19.** Variation of completeness factor versus *V* magnitude and radius for Be 24 and Cz 27.

Figure 20. Luminosity function of clusters Be 24 and Cz 27 under present study.

probable cluster members selected from VPD as shown in Fig. 5. It is necessary to clearly separate field stars from the cluster sequence for the construction of correct LF. So, we have collectively used proper motion and photometric criteria for the selection of probable cluster members. The photometric criterion adopted in Section 5 by plotting the blue and red envelope along the MS was used for selection of cluster members in the *V* versus $(V - I)$ CMD of cluster field region (see Fig. 15). Stars are counted within this envelope, for both cluster and field region. The difference between the counts in two fields after accounting for the difference in area between the cluster and field regions will be the observed cluster LF. For the construction of LFs, first we have transformed the apparent *V* magnitudes into the absolute magnitudes by using the distance modulus of the clusters. Then, we have built the histogram of LFs for the clusters as shown in Fig. 20. The interval of 1.0 mag was chosen so that there would be enough stars per bin for good statistics. The histogram shows that a dip is found at $M_V = 1.0$ mag for the cluster Cz 27. The LF for the cluster Be 24 rises steadily up to $M_V = 4.0$ mag.

6.3 Mass function

The LF can be transformed into the mass function (MF) using a mass–luminosity relation. Since we could not obtain an empirical transformation, so we rely on theoretical models.

Using the cluster parameters derived in this paper and theoretical models given by Girardi et al. (2000), we have converted the LF into an MF. To convert LFs derived in Section 6.2 into MFs, we divide the cluster members by the mass interval of the magnitude bin under consideration. The value of mass interval was obtained from the mass–luminosity relation derived from the appropriate isochrone.
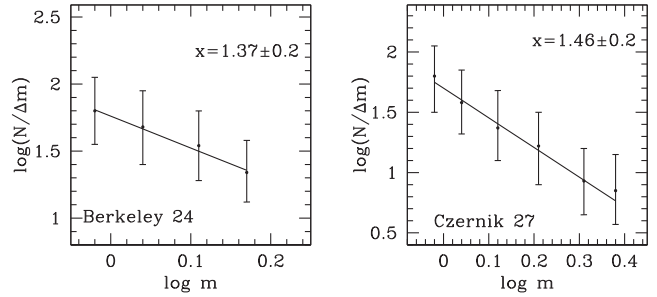

Figure 21. Mass function for Be 24 and Cz 27 derived using Girardi et al. (2000) isochrones. The error bars represent $\frac{1}{\sqrt{(N)}}$.

The resulting MF for both the clusters are shown in Fig. 21. The mass function slope can be derived from the linear relation

$$\log \frac{dN}{dM} = -(1 + x) \times \log(M) + \text{constant}$$

using the least-squares solution. In the above relation, d*N* represents the number of stars in a mass bin d*M* with central mass *M* and *x* is the mass function slope. The Salpeter (1955) value for the mass function slope is $x = 1.35$.

The derived mass function slope is $x = 1.37 \pm 0.2$ and 1.46 ± 0.2 for the clusters Be 24 and Cz 27, respectively. The overall MF slope for both the clusters are in good agreement with the Salpeter value $(x = 1.35)$ within errors. The mass is calculated by considering overall mass function slope with in the mass range $0.9 - 1.6$ $M_\odot$ for Be 24 and $0.9 - 2.4$ $M_\odot$ for Cz 27. Total mass was estimated as ~ 80 $M_\odot$ and ~ 84 $M_\odot$ for clusters Be 24 and Cz 27, respectively.

There are many MF studies available in the literature using open star clusters in the Milky Way. Piskunov et al. (2004) studied five young open star clusters and found that stellar mass function of these clusters are well represented with a power law, very similar to Salpeter value within the uncertainties. MF study of Phelps & Janes (1993) using a sample of seven star clusters also conclude the Salpeter type MF slope in these clusters. Sanner & Geffert (2001), Sagar (2001), and Yadav & Sagar (2002, 2004) also found consistent with the Salpeter value.

7 DYNAMICAL STATE OF THE CLUSTERS

To study the effect of mass segregation on the clusters, we plot the cumulative radial stellar distribution of stars for different masses in Fig. 22. To bring out the mass segregation effect, we have divided the main sequence stars in three mass ranges, $1.6 \leq \frac{M}{M_\odot} \leq 1.5$, $1.5 \leq \frac{M}{M_\odot} \leq 1.2$, and $1.2 \leq \frac{M}{M_\odot} \leq 0.9$ for Be 24 and $2.4 \leq \frac{M}{M_\odot} \leq 1.7$, $1.7 \leq \frac{M}{M_\odot} \leq 1.2$, and $1.2 \leq \frac{M}{M_\odot} \leq 0.90$ for Cz 27. To study the cluster dynamical evolution and mass-segregation effect, we selected probable members based on VPD and CMD of the clusters Be 24 and Cz 27. The cumulative distributions shown in Fig. 22 are also corrected for the incompleteness as listed in Table 7 and field star contamination. This figure clearly exhibits mass-segregation effect, in the sense that massive stars gradually sink towards the cluster centre than the fainter stars. To check whether these mass distributions represent the same kind of distribution or not, we have performed Kolmogorov–Smirnov (K–S) test. This test indicates that the confidence level of mass-segregation effect is 92 per cent for Be 24 and 90 per cent for Cz 27.

Furthermore, it is important to know whether the effect mass-segregation is due to dynamical evolution or imprint of star for-

Table 8. Derived fundamental parameters of the clusters under study. R_{GC} is the Galactocentric distance while $X_{\odot}$, $Y_{\odot}$, and $Z_{\odot}$ are the Galactocentric coordinates of the clusters. The coordinate system is such that the *Y*-axis connects the Sun to the Galactic Centre, while the *X*-axis is perpendicular to that. $Y_{\odot}$ is positive towards the Galactic anticentre, and $X_{\odot}$ is positive in the first and second Galactic quadrants (Lynga 1982).

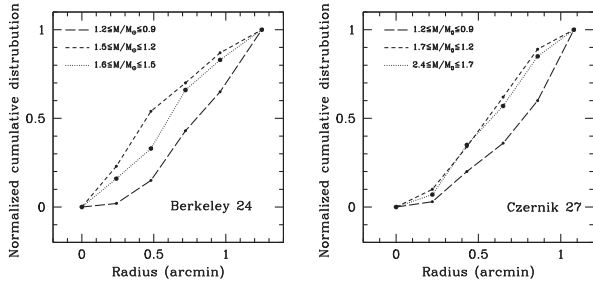| Name	Radius (arcmin)	$E(B-V)$ (mag)	Distance (kpc)	$X_{\odot}$ (kpc)	$Y_{\odot}$ (kpc)	$Z_{\odot}$ (kpc)	R_{GC} (kpc)	Age (Gyr)
Be 24	2.7	0.45 ± 0.05	4.4 ± 0.5	-0.7	12.8	-0.2	12.8	2 ± 0.2
Cz 27	2.3	0.15 ± 0.05	5.6 ± 0.2	-0.7	14.0	0.5	14.1	0.6 ± 0.1

Figure 22. The cumulative radial distribution of stars in various mass range.

mation or both. In the lifetime of star clusters, encounters between its member stars gradually lead to an increased degree of energy equipartition throughout the clusters. In this process, the higher mass cluster members accumulate towards the cluster centre and transfer their kinetic energy to the more numerous lower mass stellar component, thus leading to mass segregation.

7.1 The relaxation time of clusters

The time-scale in which a cluster will loose all traces of its initial conditions is well represented by its relaxation time T_E. The relaxation time is the characteristic time-scale for a cluster to reach some level of energy equipartition. The relaxation time given by Spitzer & Hart (1971) stated that;

$$T_E = \frac{8.9 \times 10^5 N^{1/2} R_h^{3/2}}{<m>^{1/2} \log(0.4N)},$$

where N is the number of cluster members, R_h is half-mass radius of the cluster and $<m>$ is mean mass of the cluster stars (Spitzer & Hart 1971). We identified 59 and 54 stars as probable cluster members for Be 24 and Cz 27, respectively, based on proper motion and photometric criteria. The value of $<m>$ is found as 1.35 $M_{\odot}$ and 1.55 $M_{\odot}$ for clusters Be 24 and Cz 27, respectively. The value of R_h has been assumed as half of the cluster radius derived by us. Using the above relation, we have estimated the dynamical relaxation time T_E as 9.5 and 8.0 Myr for Be 24 and Cz 27, respectively. A comparison of cluster age with its relaxation time indicates that relaxation time is smaller than the age of these clusters. Therefore, we conclude that both the clusters are dynamically relaxed.

8 CONCLUSIONS

We have studied the two open star clusters Be 24 and Cz 27 using *UBVI* CCD, *2MASS JHK*, and *GAIA DR*2 data. The results are summarized in Table 8. The main findings of our analysis are as follows:

(i) The radii of the clusters are obtained as $2\!.\!7$ and $2\!.\!3$, which correspond to 3.4 and 3.2 pc, respectively, at the distance of the clusters Be 24 and Cz 27.

(ii) From the TCD, we have estimated $E(B-V) = 0.45 \pm 0.05$ mag for Be 24 and 0.15 ± 0.05 mag for Cz 27. The *JHK* data in combination with the optical data provide $E(J-K) = 0.23 \pm 0.03$ mag and 0.06 ± 0.02 mag while $E(V-K) = 1.23 \pm 0.02$ mag and $E(V-K) = 0.33 \pm 0.01$ mag for Be 24 and Cz 27, respectively. Hence, our analysis indicates that interstellar extinction law is normal towards both clusters.

(iii) The metallicities of the clusters obtained from *UBV* photometric data are found to be [Fe/H] $= -0.025 \pm 0.01$ dex and -0.042 ± 0.01 dex for Be 24 and Cz 27, respectively. These are the first metallicity measurements for these two clusters.

(iv) Distances to the clusters Be 24 and Cz 27 are determined to be 4.4 ± 0.5 and 5.6 ± 0.2 kpc, respectively. These distances are supported by the distance values derived using parallax and optical and near-IR data. Ages of 2.0 ± 0.2 Gyr and 0.6 ± 0.1 Gyr are estimated for Be 24 and Cz 27 by comparing with the isochrones for $Z = 0.01$ given by Girardi et al. (2000).

(v) The mean proper motion was estimated to be 1.25 ± 0.09 mas yr^{-1} and 1.40 ± 0.05 mas yr^{-1} for the clusters Be 24 and Cz 27, respectively.

(vi) The luminosity function is determined by considering probable cluster members based on VPD and photometric criteria. For the cluster Cz 27, a dip is found at $M_V = 1.0$ mag and then it rises. The reason for the presence of dip a in the main sequence of the cluster is not known.

(vii) The overall mass function slopes $x = 1.37 \pm 0.2$ and 1.46 ± 0.2 are derived for Be 24 and Cz 27 by considering the corrections of field star contamination and data incompleteness.

(viii) Evidence for the mass-segregation effect was found for both clusters using probable cluster members. The K–S test shows that the confidence level of mass-segregation effect is 92 per cent and 90 per cent for Be 24 and Cz 27, respectively. Dynamical relaxation time indicates that both the clusters are dynamically relaxed. This may be due to the dynamical evolution.

REFERENCES

Ann H. B., Lee S. H., 2002, J. Korean Astron. Soc., 35, 29
Becker W., Stock J., 1954, Ze. f. Astrophys., 34, 1
Becker W., Fenkart R., 1971, A&AS, 4, 241
Bellazzini M., Pecci F. F., Messineo M., 2002, AJ, 123, 1509
Bonatto C., Bica E., 2009, MNRAS, 397, 1915
Bonnell I. A., Davies M. B., 1998, MNRAS, 295, 691
Gaia Collaboration et al., 2018, A&A, 616, 22
Caldwell J. A. R., Cousins A. W. J., Ahlers C. C., van Wamelen P., Maritz E. J., 1993, SAAO Circ., 15, 1
Cardelli J. A., Clayton G. C., Mathis J. S., 1989, ApJ, 345, 245
Carraro G., Beletsky Y., Marconi G., 2013, MNRAS, 428, 502
Chini R., Wargue W. F., 1990, A&A, 227, 5
Czernik M., 1966, AcA, 16, 92
Dias W. S., Alessi B. S., Moitinho A., Lepine J. R. D., 2002, A&A, 389, 871
Eggen O. J., 1993, AJ, 106
Genzel R., Townes C. H., 1987, ARA&A, 25, 377
Girardi L., Bressan A., Bertelli G., Chiosi C., 2000, A&AS, 141, 371
Hur H., Sung H., Bessell M. S., 2012, AJ, 143, 41
Janes K., Alder D., 1982, ApJS, 49, 425
Karaali S., Bilir S., Karatas Y., Ak S. G., 2003, PASA, 20, 165
Karaali S., Bilir S., Tuncel S., 2005, PASA, 22, 24
Karaali S., Bilir S., Ak S., Yaz E., Coskunoglu B., 2011, PASA, 28, 95
Khalaj P., Baumgardt H., 2013, MNRAS, 434, 3236
Kim S. S., Figger D. F., Lee H. M., Morris M., 2000, ApJ, 545, 301
Kim S. S. et al., 2005, J. Korean Astron. Soc., 38, 429
King I., 1962, AJ, 67, 471
Koposov S. et al., 2008, A&A, 486, 771
Kumar B., Sagar R., Rautela B. S., Srivastava J. B., Srivastava R. K., 2000, Bull. Astron. Soc. India, 28, 675
Landolt A. U., 1992, AJ, 104, 340
Lynga G., 1982, A&A, 109, 213
Maciejewski G., Niedzielski A., 2007, A&A, 467, 1065
Magrini L., Sestito P., Randich S., Galli D., 2009, A&A, 494, 95
Mathis J. S., 1990, ARA&A, 28, 37
Melnikov S., Eisl'offel J., 2012, A&A, 544, 111
Mowlavi N., Eggenberger P., Meynet G., Ekstrom S., Georgy C., Maeder A., Charbonnel C., Eyer L., 2012, A&A, 541, A41
Neckel T., Chini R., 1981, A&A, 45, 451
Ortolani S., Bica E., Barbuy B., 2005, A&A, 437, 531
Persson S. E., Murphy D. C., Krzeminski W., Roth M., Rieke M. J., 1998, AJ, 116, 2475
Peterson C. J., King I. R., 1975, AJ, 80, 427
Phelps R. L., Janes K. A., 1993, AJ, 106, 1870
Piatti A. E., Claria J. J., Ahumada A. V., 2010, MNRAS, 402, 2720
Piskunov A. E., Belikov A. N., Kharchenko N. V., Sagar R., 2004, MNRAS, 349, 1449
Romanishim W., Angel J. R. P., 1980, ApJ, 235, 992
Sagar R., 2001, IAU Circ., 207, 515
Sagar R., Griffiths W. K., 1998, MNRAS, 299, 777
Salpeter E. E., 1955, ApJ, 121, 161
Sanner J., Geffert M., 2001, A&A, 370, 87
Scalo J. M., 1986, Fund. Cosmic Phys., 11, 1
Scalo J. M., 1998, in Gilmore G., Parry I., Ryan S., eds, ASP Conf. Ser. Vol. 142, The Stellar Initial Mass Function. Astron. Soc. Pac., San Francisco, p. 201
Schmidt-Kaler Th., 1982, in Scaitersk K., Voigt H. H., eds, Landolt/Bornstein, Numerical Data and Functional Relationship in Science and Technology, New series, Group VI, Vol. 2b. Springer-Verlag, Berlin, p. 14
Skrutskie M. F. et al., 2006, AJ, 131, 1163
Sneden C., Gehrz R. D., Hackwell J. A., York D. G., Snow T. P., 1978, ApJ, 223, 168
Spitzer L., Hart M. H., 1971, ApJ, 164, 399
Stetson P. B., 1987, PASP, 99, 191
Stetson P. B., 1992, in Warrall D. M., Biemesderfer C., Barnes J., eds, ASP Conf. Ser. Vol. 25, Astronomical Data Analysis Software and System I. Astron. Soc. Pac., San Francisco, p. 297
Wilner D. J., Lada C. J., 1991, AJ, 102, 1050
Yadav R. K. S., Sagar R., 2002, MNRAS, 337, 133
Yadav R. K. S., Sagar R., 2004, MNRAS, 349, 1481

This paper has been typeset from a TEX/LATEX file prepared by the author.